Detonation Performance of a High HMX-Content Polymer Bonded Explosive

Eric K. Anderson, Stephen J. Voelkel, Mark Short, Ritchie I. Chicas,
Wesley W. Chapman, Carlos Chiquete
Shock and Detonation Physics, Los Alamos National Laboratory,
Los Alamos, NM 87544, USA

1 Introduction

Polymer bonded explosives (PBXs) were designed in the 1950s and bind explosive crystal material within a polymer matrix, and intended to provide good explosive performance properties, while maintaining desirable chemical and mechanical stability properties. A number PBXs use cyclotetramethylene-tetranitramine (HMX) as the explosive crystal. Binders used in combination with HMX have include various fluoropolymers, elastomers and energetic polymers, or combinations thereof. Several HMX-based PBXs have been developed with varying HMX weight percentage (wt.%) content, including PBX 9012 (90 wt.% HMX), LX-07 (90 wt.% HMX), EDC-37 (91 wt.% HMX), PBX 9404 (94.0 wt.% HMX), PBX 9501 (95.0 wt.% HMX), and LX-14 (95.5 wt.% HMX).

PBX 9751 (also known as X-0298) is a high-HMX content HE consisting of 97.5 wt.% HMX, with a binder consisting of 1.12 wt.% Kraton G-1650 and 1.38 wt.% paraffinic oil [1]. It was developed as a high HMX wt.% alternative to PBX 9501. Kraton G-1650 is a styrene-ethylene-butylene-styrene block coploymer noted for its thermal and chemical stability, while paraffinic oil increases the elasticity and reduces the tensile modulus of Kraton, as described in [1]. The pressing density of PBX 9751 is 1.813-1.825 g/cc. It has been shown to possess good safety properties relative to PBX 9404 and PBX 9501 [1].

In this work, we investigate the detonation performance of PBX 9751. Detonation speeds and shock shapes from 6 cylindrical rate-stick geometry tests are used to calibrate a detonation shock dynamics (DSD) model. Additionally, a copper cylinder expansion (CYLEX) test is used to determine a Jones-Wilkins-Lee (JWL) EOS for PBX 9751 products. The detonation performance properties of PBX 9751 are then compared to those of the lower HMX-content HE PBX 9012, which has been previously characterized using similar experimental and analysis techniques [2].

2 Rate-stick experiments and Detonation Shock Dynamics Modeling

Six cylindrical rate-stick tests were performed on PBX 9751 (Fig. 1). Dimensions are shown in table 1. The tests were conducted using the same experimental procedures described in [2, 3]. Figure 2 shows the diameter effect and diameter chord arrival times on the breakout surface of the HE for each test.

Correspondence to: eanderson@lanl.gov

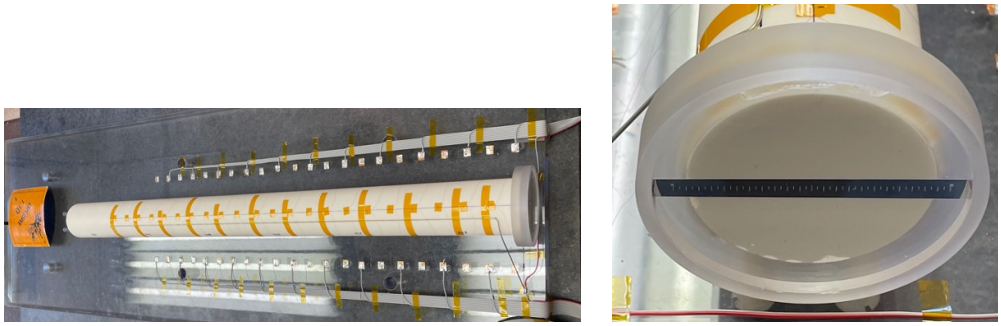

Figure 1: Left (L): Rate-stick assembly for a PBX 9751 test. Right (R): Mirror and fiducial assembly for detonation shock arrival time measurements along a diameter chord at the end of charge [2].

Table 1: Rate-stick test data. Here, d is the rate-stick diameter, D_0 is the steady detonation axial propagation speed and ρ_0 is the initial density.

Shot Number	d (mm)	ρ_0 (g/cm^3)	D_0 (mm/μs)	Std. Error D_0 (m/s)
8-2308	50.08	1.813	8.830	1.0
8-2341	25.41	1.815	8.822	3.0
8-2307	10.19	1.814	8.817	5.0
8-2316	5.71	1.812	8.783	1.0
8-2317	3.89	1.815	8.750	3.0
8-2318	2.97	1.814	8.699	3.0

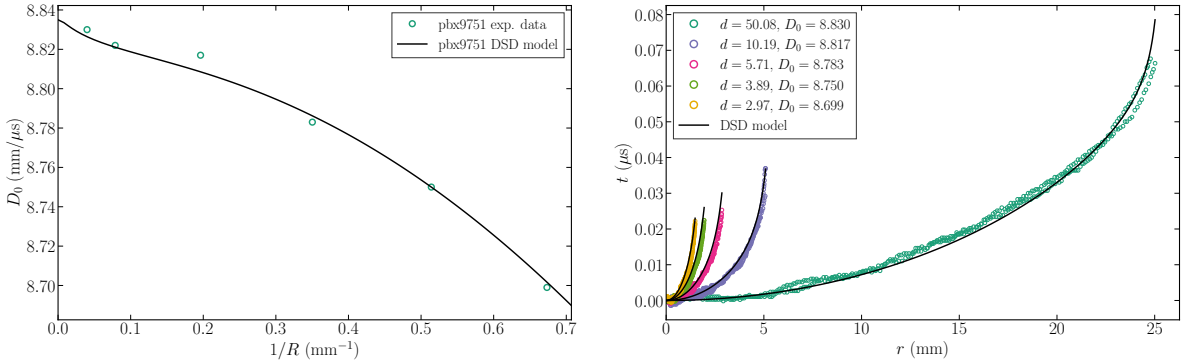

Figure 2: (Left) Diameter effect and (Right) diameter chord arrival time for each d. Also shown is the DSD model calibration of PBX 9751 illustrating comparisons of the fitted diameter effect and diameter chord arrival times.

A Detonation Shock Dynamics (DSD) model for detonation motion in PBX 9751 was calibrated from the experimental diameter effect and diameter chord arrival time data. The DSD surface motion model assumes that the normal speed of the surface (D_n) at any point on the surface is a function of its local curvature (κ) [4]. The functional form of the $D_n - \kappa$ relationship we used for PBX 9751 is given by

$$D_n(\kappa) = D_{CJ}\left[1 - B\kappa\left(\frac{1 + C_2\kappa + C_3\kappa^2}{1 + C_4\kappa}\right)\right], \tag{1}$$

where D_{CJ} is the CJ detonation velocity and B, C_2, C_3, and C_4 are function parameters to be calibrated, along with the angle ϕ_e between the DSD surface normal and the axial direction at the edge of the HE [2, 3]. A Nelder-Mead merit function minimization procedure [5] was used to fit the DSD model parameters to both the diameter effect and diameter chord arrival time records.

Table 2: PBX 9751 DSD model parameters.

D_{CJ} (mm/μs)	ϕ_e (deg)	B (mm)	C_2 (mm)	C_3 (mm)	C_4 (mm)
8.835	25.0	0.623562	21.853476	8.924220	271.894897

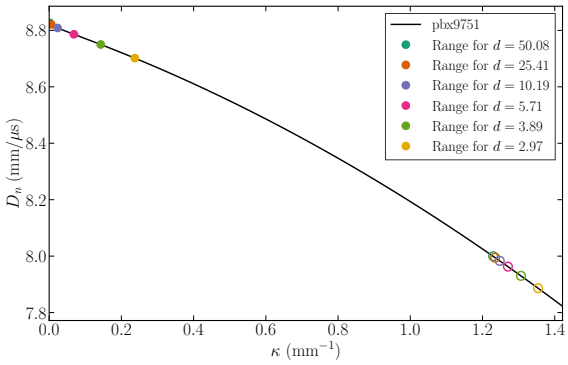

Figure 3: $D_n - \kappa$ variation for PBX 9751 derived from the fitted DSD models.

Table 2 gives the optimized DSD model parameters. Figure 2 shows the DSD model calibration fits of the diameter effect and diameter chord arrival times. Figure 3 shows the DSD model-based $D_n - \kappa$ variation for PBX 9751. The PBX 9751 DSD model calibrated Chapman-Jouguet speed is 8.835 mm/μs and compares to a value of 8.590 mm/μs for the 90 wt.% HMX-based HE PBX 9012, a difference of 245 m/s [2]. The $D_n - \kappa$ relation in Fig. 3 is typical of a conventional HE, where large κ values are needed to observe a significant drop in D_n.

3 JWL Products EOS

A CYLEX test was also conducted to calibrate the JWL product equation-of-state (EOS) for PBX 9751. The procedures were identical to that described in [6]. The HE and Cu tube dimensions are shown in table 3. The axial detonation speed and diameter chord arrival time fields were also recorded. Eight collimated PDV probes were used to measure the motion of the copper (Cu) wall at various positions on the Cu tube [6]. Figure 4L shows the PDV probe velocity histories in the radial direction of the Cu wall expansion. The PDV probe velocity histories can be averaged by forming an arithmetic mean of the velocity histories at each $t - t_0$. This average is shown in Fig. 4R.

As described in [6], the JWL EOS is of Mie-Grüneisen form and is based on a reference curve describing the pressure (p_s) variation with volume (v) along the principal isentrope, where

$$p_s = A \exp\left[-R_1 v/v_0\right] + B \exp\left[-R_2 v/v_0\right] + C(v/v_0)^{-1-\omega}, \tag{2}$$

where C is a label parameter for the principal isentrope, v_0 ($= 1/\rho_0$) is the initial specific volume of the HE, and A, R_1, B, R_2 and ω are the JWL EOS parameters, with $R_1 > R_2$. For states off the principal isentrope, the EOS form is

$$p = p_s + \omega(e - e_s)/v, \quad e_s = \int_v^\infty p_s \, dv. \tag{3}$$

As described in [6], the area under the isentrope from $v = v_{CJ}$ to $v = \infty$ minus the area under the Rayleigh line from $v = v_0$ to $v = v_{CJ}$ ($v_{CJ} < v_0$) defines the heat of detonation e_0, such that

$$e_0 = e_s(v_{CJ}) - p_{CJ}(v_0 - v_{CJ})/2. \tag{4}$$

Table 3: CYLEX test data. Here, Cu ID and Cu OD denote the inner and outer diameter of the copper tube, respectively.

Shot Number	d (mm)	Cu ID (mm)	Cu OD (mm)	ρ_0 (g/cm^3)	D_0 (mm/μs)	Std. Error D_0 (m/s)
8-2331	25.40	25.44	30.48	1.813	8.816	1.0

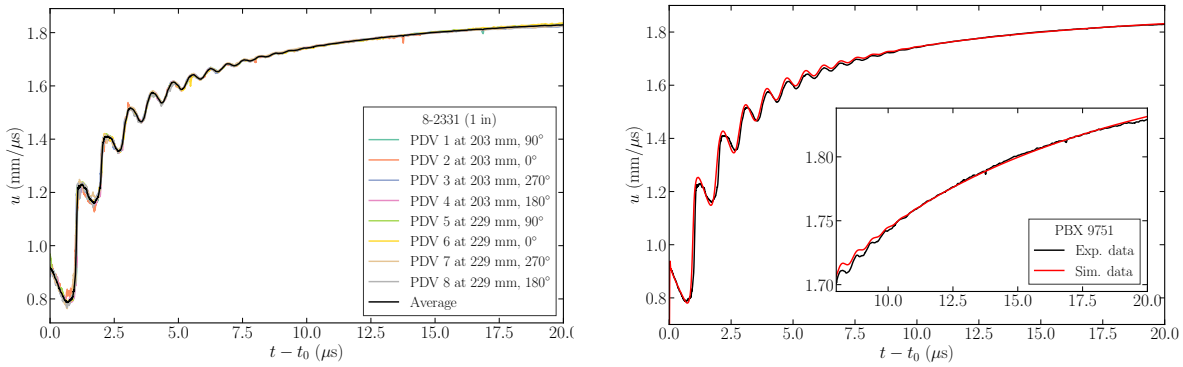

Figure 4: L: Radial component of the outer Cu wall velocity (u) with time (t) relative to the time of wall motion start (t_0) for the various PDV probe axial positions and angles shown. Also plotted is the velocity-time trace of the averaged PDV probe data. R: Comparison of the averaged PDV probe radial velocity field with the simulated wall motion based on the calibrated JWL EOS model (Table 4).

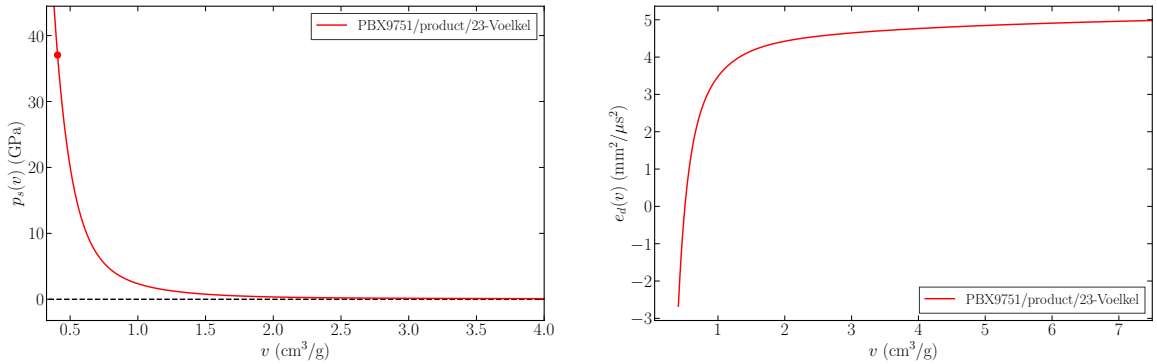

Figure 5: L: The JWL product principal isentrope for PBX 9751. The circle indicates the CJ state. R: Detonation product work variation $e_d(v) = e_0 - e_s(v)$.

The evolution in the detonation work with volume going from $v = v_{CJ}$ to any v is given by $e_d(v) = e_0 - e_s(v) = e_s(v_{CJ}) - e_s(v) - p_{CJ}(v_0 - v_{CJ})/2$, so that $e_d(v_{CJ}) = -p_{CJ}(v_0 - v_{CJ})/2$ and $e_d(v \to \infty) = e_0$.

The numerical JWL product EOS calibration process follows that described in [6], where the simulated and experimentally measured Cu wall radial expansion profiles, i.e. the averaged PDV profiles shown in Fig. 4L, are compared, and A, B, R_1, R_2 and ω then iterated on to provide the desired level of fit. Table 4 shows the resulting JWL product EOS parameters for PBX 9751, along with the corresponding heat of detonation e_0. Figure 4R shows a comparison of the averaged experimental PDV probe radial velocity fields with the simulated wall motions based on the calibrated JWL EOS model. The principal isentrope variation for the PBX 9751 detonation products is shown in Fig. 5L. The corresponding variation in the detonation product work e_d with volume is shown in Fig. 5L.

Table 4: JWL product EOS parameters for PBX 9751, along with the corresponding heat of detonation e_0 and detonation work e_d at varied volumes.

A (GPa)	B (GPa)	R_1	R_2	ω	e_0 (mm^2/μs^2)
828.251497	22.208781	4.614384	1.466108	0.344186	5.873423

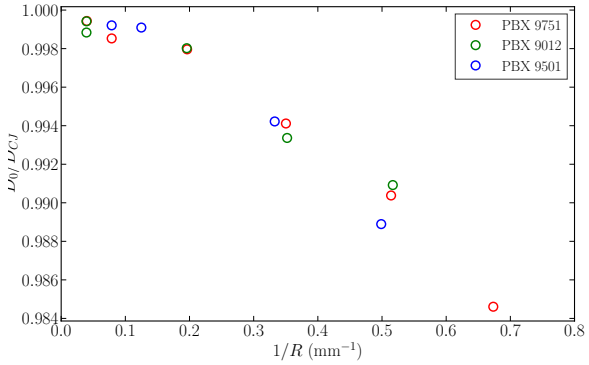

Figure 6: Diameter effect curves for PBX 9012 and PBX 9751, with D_0 scaled by D_{CJ} for each HE. Also shown is 95.0 wt.% HMX PBX 9501 data from [7].

4 Comparison with PBX 9501 and PBX 9012

In [2], a study was conducted on the comparative effect of HMX content on the detonation performance of PBX 9012 (90.0 wt.% HMX) and PBX 9501 (95.0 wt.% HMX). We can now add PBX 9751 (97.5 wt.% HMX) to this analysis. Figure 6 shows the diameter effect curves for PBX 9012, PBX 9501 and PBX 9751, with D_0 scaled by D_{CJ} for each HE. The similar behavior of the scaled curves indicates that the first order effect of increasing the HMX content on the diameter effect appears to be an overall increase in the energy available for propagation. Moreover, comparing the $D_n - \kappa$ curves for PBX 9751 and PBX 9012, when D_n for each HE is scaled by its D_{CJ}, the curves lie close together. This indicates that the relative length scales of reaction in PBX 9012 and PBX 9751 are similar, despite the higher HMX content of PBX 9751. Additionally, when the CYLEX test wall trajectories are compared between PBX 9751 and PBX 9012, again scaled by D_{CJ} for each HE, the trajectories are similar. Finally, the heats of detonation when scaled by D_{CJ}^2 for each HE are also similar.

5 Summary

PBX 9751 is a 97.5 wt.% HMX-based HE with excellent stability properties due to its Kraton binder system. We have conducted a complete detonation performance assessment of PBX 9751, including the calibration of DSD/JWL models. PBX 9751 has higher detonation performance characteristics than the lower HMX-content HEs PBX 9012 and PBX 9501. However, the relative content of HMX seems to be strongly underlie the detonation performance characteristics.

References

[1] T.M. Benziger, E.D. Loughran, and R.K. Davey. X-0298: a rubber-bonded PBX.[rubber-bonded HMX]. Technical Report LA-8436-MS, Los Alamos National Lab.(LANL), Los Alamos, NM (United States), 1980.

[2] E.K. Anderson, C. Chiquete, S.I. Jackson, R.I. Chicas, and M. Short. The comparative effect of HMX content on the detonation performance characterization of PBX 9012 and PBX 9501 high explosives. *Combust. Flame*, 230:111415, 2021.

[3] C. Chiquete, M. Short, E.K. Anderson, and S.I. Jackson. Detonation shock dynamics modeling and calibration of the HMX-based conventional high explosive PBX 9501 with application to the two-dimensional circular arc geometry. *Combust. Flame*, 222:213–232, 2020.

[4] J.B. Bdzil and D.S. Stewart. The dynamics of detonation in explosive systems. *Annu. Rev. Fluid Mech.*, 39:263–292, 2007.

[5] J.A. Nelder and R. Mead. A simplex method for function minimization. *The Computer Journal*, 7:308–313, 1965.

[6] S.J. Voelkel, E.K. Anderson, M. Short, C. Chiquete, and S.I. Jackson. Effect of microstructure on detonation performance of the triaminotrinitrobenzene (TATB)-based insensitive high explosive PBX 9502. *Combust. Flame,*, 246:112373, 2022.

[7] S.I. Jackson and M. Short. Scaling of detonation velocity in cylinder and slab geometries for ideal, insensitive and non-ideal explosives. *J. Fluid Mech.*, 773:224–266, 2015.